

Preparation and Electrocapacitive Properties of Hierarchical Porous Carbons Based on Synthesized 1,3,5-tris (1-imidazolyl) benzene

Zichao Li¹, Kuilu Zhai², Peng Xu², Yue Wang^{2,*}, and Qun Li^{2,*}

¹ College of Life Sciences, Qingdao University, Qingdao 266071, China; zichaoli@qdu.edu.cn (Z.L.)

² College of Chemistry and Chemical Engineering, Qingdao University, Qingdao 266071, China; zhaikuilu@gmail.com (K.Z.); 2017020860@qdu.edu.cn (P.X.)

*E-mail: qunli@qdu.edu.cn (Q.L.); wangyue@qdu.edu.cn (Y.W.)

Received: 14 May 2018 / Accepted: 11 June 2018 / Published: 5 August 2018

In this paper, we report the preparation of four porous carbons denoted as TC-1, TC-2, TC-3, and TC-4 based on synthesized 1,3,5-tris (1-imidazolyl) benzene (tib) through carbonization at different temperatures under inert gas atmosphere and their electrocapacitive properties for supercapacitor applications. The specific surface areas of as-made TCs were 309, 419, 305 and 73 m²/g mainly with micropores, respectively. The results of electrochemical tests show quasi-rectangular shapes of all the cyclic voltammeteries of the four supercapacitors (SC-TCs), even under a high scan rate of 500 mV·s⁻¹. The specific capacitances of SC-TCs at 0.1 A·g⁻¹ were 88.5, 102.1, 101.9 and 18.3 F·g⁻¹, respectively in 6 M KOH solutions. The structure-property relationship of TCs is discussed and analyzed on the basis of the experimental data. Our results provide a novel route for the preparation of porous carbon materials from synthesized benzene-contained organic compounds and exhibit the potentiality for application in energy storage.

Keywords: 1,3,5-tris (1-imidazolyl) benzene; porous carbon; carbonization; capacitance; hydrothermal synthesis

1. INTRODUCTION

The fast development of human society highly demands sustainable energy and advanced energy technologies to date. For instance, the rapid-growing markets of portable electronics and hybrid electric vehicles are causing an urgent need for eco-friendly high-power energy resources. Supercapacitors has been reported to be ideal power sources due to their high power density, long lifecycle, environmental friendliness and safety, compared with lithium batteries [1,2], and have attracted enormous attentions for their multiple applicable possibilities in industries, especially in the

hybrid electrical vehicles field [3,4]. Combined with batteries or fuel batteries, supercapacitors exhibit a better performance in high power supply during acceleration, energy recovery during braking, excellent cold weather starting and increased battery life [2,5]. Supercapacitors are likely to complement or even replace batteries for energy conversion and storage field in future [6].

Carbon materials are widely used as electrode materials due to their distinct properties including low cost, easy processing, eco-friendliness, good electronic conductivity, high chemical stability, and wide operating temperature range [7]. Activated carbons with large surface area and controllable pore size are the most commonly used electrode materials. It is well known that a large surface area is essential for the double layer charge accumulation [8,9]. Moreover, the pore size distribution plays a crucial role on electrode performance. Further studies demonstrated that micropores were more capable of charge accumulation due to the high energy density [10,11]. Moreover, mesopores are necessary for the rapid charge propagation which can contribute to high power density [12,13]. Hence, porous carbons with effective combination of micropores and mesopores can achieve both the high energy and power density. Although the template method can achieve the preparation of activated carbons with relatively good electrochemical performance, the high cost limits its practical application [14]. Changing the process parameters such as precursors, activation agent, and activation temperature is an efficient way to obtain activated carbons with better application performance [4,15,16].

1,3,5-tris (1-imidazolyl) benzene (tib) has been previously reported as a useful ligand for metal organic frameworks (MOFs) construction with specific structures, topologies and interesting properties. Tib, known as a tripodal and rigid ligand of planar type, is considered to be easily formed hierarchical structures [17-19]. Our previous study reported four loofah sponge-based porous carbons prepared via various strategies with good electrochemical properties and the results indicated the carbon materials containing nitrogen element or benzene structure might be promising carbon precursors to prepare activated carbons [4]. In this paper, by designing the unique molecular structure, tib was synthesized through a simple strategy and hierarchical porous carbon materials based on which were prepared via carbonization at controlled temperatures. The results show that the porous carbons carbonized at 600 °C possessed the largest specific surface area among the four prepared samples, and the highest specific capacitance of 102.1 F·g⁻¹ at 0.1 A·g⁻¹ in symmetrical supercapacitors with 6 M KOH solutions as the electrolyte. And except for the sample carbonized at 800 °C, all the other porous carbons exhibited good electrochemical stability. Furthermore, the structure-property relationship of the tib-based porous carbons is discussed and analyzed on the basis of the experimental data.

2. MATERIALS AND METHODS

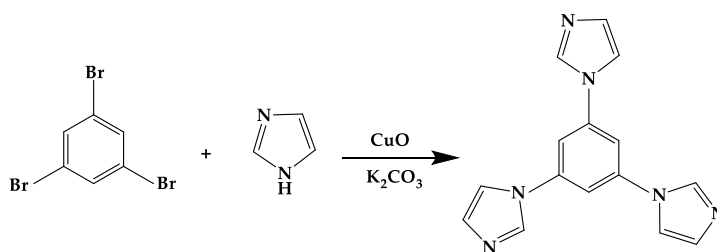
2.1. Reagents and Materials

Chemicals including CuO and anhydrous K₂CO₃ were procured from Sinopharm Chemical Reagent Co., Ltd (Shanghai, China). Imidazole, and 1,3,5-tribromobenzene were obtained from Henghua Sci. & Tec. Co., Ltd (Jinan, China). Acetylene carbon black (99.99%) and polytetrafluoroethylene latex (PTFE, 20 wt %) were purchased from Strem Chemicals, Inc. (Boston,

MA, USA) and Sigma-Aldrich Chemie GmbH (Deisenhofen, Germany), respectively. Double-distilled water and analytical grade reagents were used without further purification in all experiments.

2.2 Synthesis of tib

Prior to the carbonization process, the synthesis of tib is shown in Scheme 1. Briefly, imidazole and tribromobenzene with weight ratio 6:1 were fully mixed and ground with catalysts including CuO and anhydrous K₂CO₃, and subsequently placed into the reactor. A mixture containing over 90% tib were obtained after the reaction. Then the pure tib were finally obtained by separation with methanol.



Scheme 1. Synthesis strategy of tib.

2.3 Preparation of the tib Based-Porous Carbons (TCs)

For the carbonization of the synthesized tib, similar to our previous report [15], 15 g of prepared sample was placed in a quartz tube furnace (MXG1200-60, Micro-X Furnace Co., Ltd, Shanghai, China) and carbonized for 2 h at controlled temperatures (500 °C, 600 °C, 700 °C, and 800 °C) in argon atmosphere with the heating rate of 5 °C/min and flow rate of 60 mL/min. The obtained tib-based granular porous carbons carbonized at 500 °C, 600 °C, 700 °C, and 800 °C are denoted as TC-1, TC-2, TC-3 and TC-4, respectively.

2.4 Characterization of TCs

Thermal gravimetric analysis (TGA) and differential scanning calorimetry (DSC) were performed on a thermo-gravimetric analyzer (TGA822e, Mettler Toledo GmbH, Greifensee, Switzerland) with a pure air flow of 100 mL/min and temperature ramp of 10 °C/min. The nitrogen adsorption-desorption isotherms were measured at 77 K with an automatic volumetric sorption analyzer (Autosorb-iQ, Quantachrome Corp., Boynton Beach, FL, USA). The specific surface area was calculated based on the Brunauer Emmett and Teller (BET) equation. The pore sizes were calculated by using the density functional theory (DFT) model [20].

2.5 Electrochemical Performance

The working electrodes were prepared by mixing tib-based porous carbons, acetylene carbon black, and PTFE with a ratio of 85:10:5. The slurry was made by adding a light amount of isopropanol, and subsequently, pressed onto a nickel foam substrate with 10 mm diameter at 1.4 MPa. Then the electrodes were dried in a vacuum oven at 110 °C for 12 h. The supercapacitors were fabricated in two-electrode Swagelok cells assembled with aqueous 6 M KOH electrolyte isolated by a porous membrane. Cyclic voltammetry (CV), galvanostatic charge-discharge (GCD) and electrochemical impedance spectroscopy (EIS) tests were performed on an electrochemical workstation (CHI760e, CH Instrument Inc., Austin, TX, USA). CV tests were carried out in the voltage ranging from 0 V to 0.8 V at the scan rate from 50 mV to 500 mV. GCD tests were measured in the voltage ranging 0–1 V under different current densities. Based on the charge-discharge curves, the specific capacitance of TCs can be calculated according to the following equation [21]:

$$C = 4 \cdot I \Delta t / \Delta V m \quad (1)$$

Where I (A) is the discharge current, Δt (s) is the discharge time, ΔV is the potential window during the discharge progress after IR drop, m (g) is the total mass of TC, C (F/g) is the specific capacitance of the supercapacitor cell. EIS measurements were carried out in the frequency range from 0.01 Hz to 100 kHz with 5 mV AC amplitude.

3. RESULTS AND DISCUSSION

3.1. Characterization of TCs

The porosity properties of TCs were investigated by collecting data of N₂ sorption at 77 K. The nitrogen adsorption isotherms and the pore size distribution of TCs are summarized in Figure 1 and Table 1, respectively. All TCs exhibited a combination of type I and type II isotherms according to the IUPAC classification [22]. A high nitrogen uptake at relative pressure below 0.02 can be noticed from the isotherms and a sharp rise at P/P₀ above 0.9 which may be due to the interparticular voids of TCs [23]. As seen, the porosity of the TCs was significantly influenced by the carbonization temperatures. With the temperature increasing from 500 °C to 800 °C, the surface area reached top at 600 °C and went down to bottom at 800 °C, simultaneously with the pore volumes decreased, which can be attributed to the degradation of the carbon skeleton caused by the higher temperature [24]. Notably, for the four prepared samples, TC-2 exhibited the highest adsorption capacity and it can be inferred that the pore structure can be well adjusted by controlling the parameters such as the temperature during the carbonization, similar to our previous results [15]. Moreover, the highest surface area was 419 m²/g of TC-2 with a total pore volume of 0.79 cm³/g, which was mainly contributed by micropores. It can be clearly seen from Figure 1b that the pore distribution of all TCs was mainly below 2 nm and a considerable proportion of mesopores were also observed. The sharp distribution of micropores around 1.7 nm suggests that the TCs are potential for energy storage. It is well acknowledged that a single micropore structure will restrict the electric double-layer capacitance although it usually guarantees good capability of energy storage, thus mesopores are needed as well for the full accessibility of electrolytes in inner pores [1,2]. Combining the aforementioned factors, a predictable result of good

capacitive performance to be determined for TC-2 correlates with its suitable higher surface area and uniform pore size.

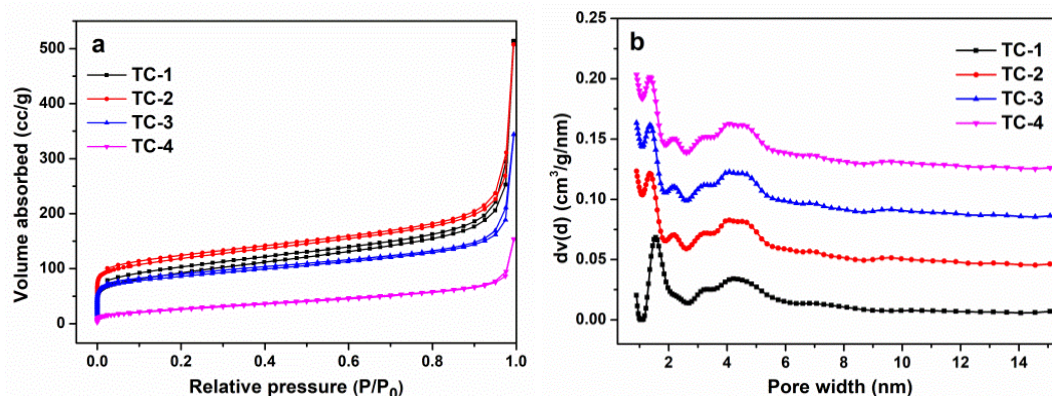


Figure 1. (a) Nitrogen adsorption–desorption isotherms and (b) pore size distributions of TCs.

Table 1. Specific surface areas, pore volumes, and pore width of TCs.

Sample	S_{BET} ($\text{m}^2 \cdot \text{g}^{-1}$)	Micropore Area ($\text{m}^2 \cdot \text{g}^{-1}$)	Micropore Volume ($\text{cm}^{-3} \cdot \text{g}^{-1}$)	V_{pore} ($\text{cm}^{-3} \cdot \text{g}^{-1}$)	Pore Width (nm)
TC-1	309	95.6	0.05	0.80	1.56
TC-2	419	221.3	0.10	0.79	0.55
TC-3	305	158.5	0.07	0.53	0.55
TC-4	73	0	0	0.24	4.22

S_{BET} : Brunauer–Emmett–Teller surface area.

The thermal behaviors for TGA and DSC of TCs at the temperature ranging from 30 °C to 800 °C were shown in Figure 2. About 10% of weight loss of all TCs at the first step can be seen from Figure 2a which can be attributed to the evaporation of minor moisture absorbed by the porous carbons. And the mass of TCs drastically decreases in the range of 420–625 °C accompanying with a large exothermic peak at around 550–600 °C on the DSC curves shown in Figure 2b, which is corresponding to the carbon oxidation in the samples [25]. No notable weight loss can be observed above 625 °C and the total weight loss of TCs all exceeds 96% indicating that the prepared samples contain only inorganic compounds and the purity of synthesized tib is high as expected.

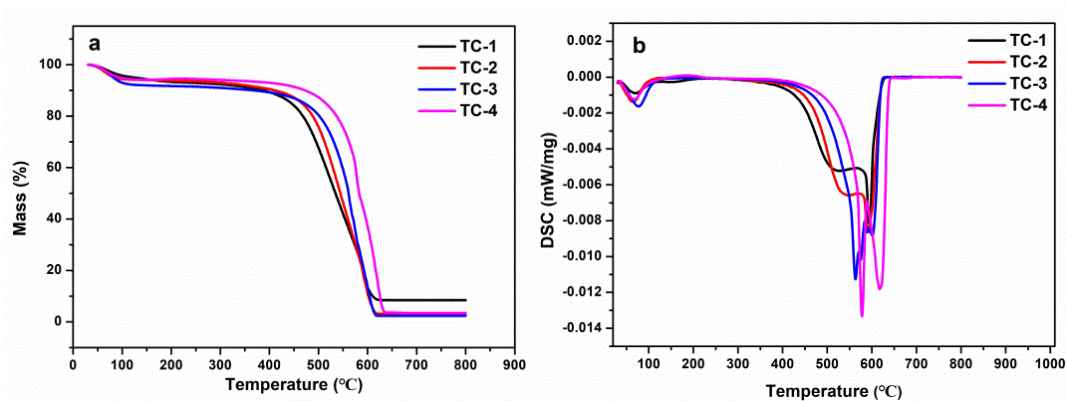
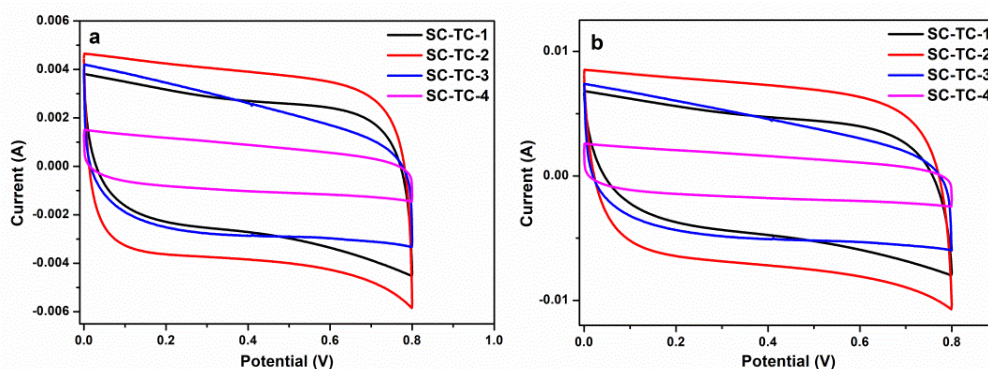


Figure 2. (a) TGA and (b) DSC profiles of TCs.

3.2. Electrochemical Characterization of TCs

The electrocapacitive properties of TC-based supercapacitors (SC-TCs), assembled from TC-1, TC-2, TC-3, and TC-4, are denoted as SC-TC-1, SC-TC-2, SC-TC-3, and SC-TC-4, respectively, and were evaluated by CV, GCD, and EIS tests in sequence at room temperature. The CV curves of SC-TCs with a potential window ranging from 0 V to 0.8 V at different scan rates are shown in Figure 3. As seen, all SC-TCs showed the quasi-rectangular shape at the relatively low scan rates (Figure 3a-3b), implying the typical capacitive behavior and ideal nature of double-layer capacitor in the charge-discharge process. And the CV profiles of SC-TCs still maintained the quasi-rectangular shape with little distortion even at the high scan rate of $500 \text{ mV}\cdot\text{s}^{-1}$, as shown in Figure 3d. It can be noticed that TC-2 was the most promising material with the best capacitance behavior by comparing with other TCs due to its highest surface area and proper hierarchical porous structure. However, for TC-1 and TC-3, they possessed lower specific surface, thus with relatively limited capacitance. Moreover, TC-4 exhibited the lowest capacitor property, as the degradation of the carbon skeleton caused by the high temperature of $800 \text{ }^\circ\text{C}$ resulted in the lowest surface area among all TCs, leading to the negative effects for mass transport. It can be inferred that both the specific surface area and uniform pore size distribution may drastically affect the capacitor performance of carbon materials.



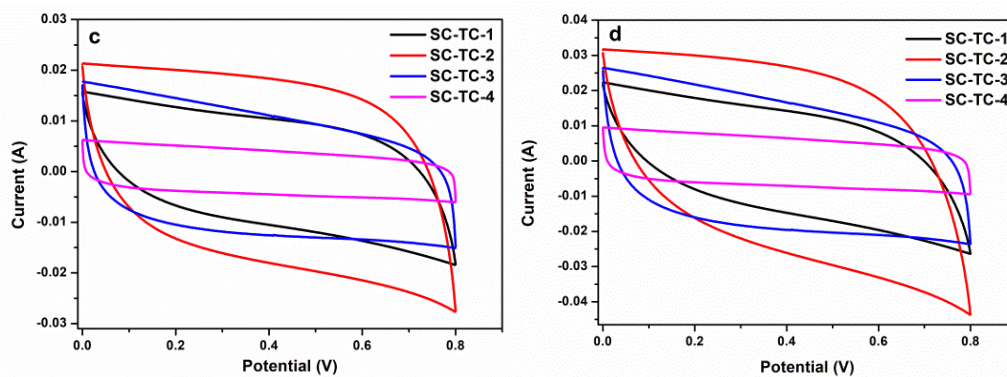


Figure 3. CV curves of SC-TCs at different scan rates ($\text{mV}\cdot\text{s}^{-1}$): (a) 50; (b) 100; (c) 300; and (d) 500.

The GCD curves of all SC-TCs at the various current densities are displayed in Figure 4. All the curves exhibit the typical isosceles triangle shape, although imperfect symmetry can be observed with a slight IR drop. The specific capacitances of the four samples calculated from the discharging curves were about 88.5, 102.1, 101.9 and 18.3 $\text{F}\cdot\text{g}^{-1}$ at the current density of $0.1\text{ A}\cdot\text{g}^{-1}$ for TC-1, TC-2, TC-3, and TC-4, respectively, which was in accordance with CV profiles. And the capacitances of SC-TCs decreased to 60.2, 78.8, 67.5 and 8.9 $\text{F}\cdot\text{g}^{-1}$, respectively, at the current density of $1\text{ A}\cdot\text{g}^{-1}$. When the current density was set at $3\text{ A}\cdot\text{g}^{-1}$, the declined capacitance of SC-TC-2 and SC-TC-3 was not significant compared with the other two SC-TCs. Furthermore, it can be seen from these results that the discharge time of SC-TC-4 was notably decreased, compared with other SC-TCs.

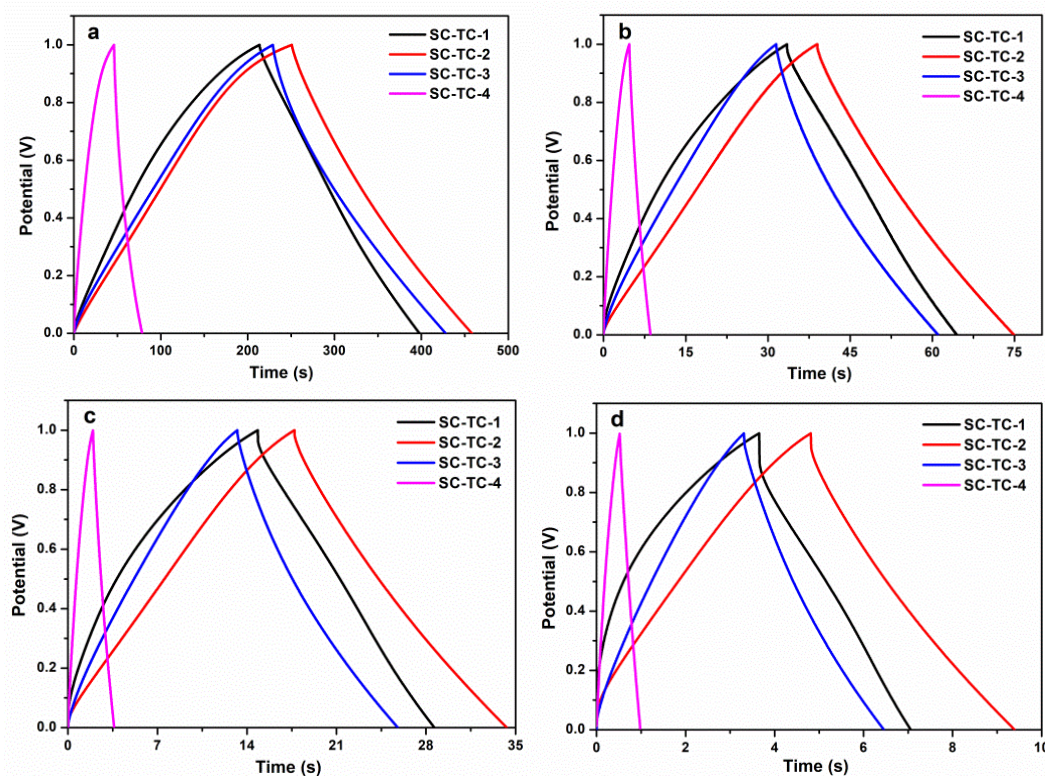


Figure 4. GCD curves of SC-TCs at different current densities ($\text{A}\cdot\text{g}^{-1}$): (a) 0.1; (b) 0.5; (c) 1; and (d) 3.

The comparison of specific capacitances among similar electrode materials for supercapacitors are listed in Table 2. It can be inferred that the simple strategy for molecular design as the carbon precursor can be efficient to prepare porous carbon materials for supercapacitor application.

Table 2. A comparison of various parameters for different activated carbon based supercapacitors.

Materials	BET surface area ($\text{m}^2 \cdot \text{g}^{-1}$)	Specific Capacitance* ($\text{F} \cdot \text{g}^{-1}$)	References
loofah sponge-based activated carbon	1007 $\text{m}^2 \cdot \text{g}^{-1}$	107	[4]
tib based porous carbon	419 $\text{m}^2 \cdot \text{g}^{-1}$	102	this work
tobacco-derived activated carbon	1298 $\text{m}^2 \cdot \text{g}^{-1}$	148	[26]
activated pinecone carbon	808 $\text{m}^2 \cdot \text{g}^{-1}$	69	[27]
activated carbon monolith	744 $\text{m}^2 \cdot \text{g}^{-1}$	90	[28]
activated carbon monolith	485 $\text{m}^2 \cdot \text{g}^{-1}$	85	[29]
hydrothermal carbonized carbon sphere	1020 $\text{m}^2 \cdot \text{g}^{-1}$	115	[30]
commercial activated carbon	1380 $\text{m}^2 \cdot \text{g}^{-1}$	90	[30]

* Calculated from GCD tests.

The variations of the specific capacitance under the different current densities of SC-TCs are shown in Figure 5a. The capacitances of SC-TCs exhibited notable decrease at the current density below $3 \text{ A} \cdot \text{g}^{-1}$. And with the current density further increased, the capacitances slightly changed, especially for SC-TC-3 and SC-TC-4. Figure 5b displays the inner resistance (IR) drop with the current density of SC-TCs, and the low values below 0.05 V were observed when the current density was less than $1 \text{ A} \cdot \text{g}^{-1}$. For SC-TC-1, SC-TC-2, and SC-TC-3, the IR drop increased with the rise of the current density, while no notable change of IR drop was observed for SC-TC-4 due to its low capacitance leading to the inability of change with the variation of current density. And except for SC-TC-1, the IR drop increased slowly to less than 0.08 V for SC-TC-2 and SC-TC-3 with the current density more than $1 \text{ A} \cdot \text{g}^{-1}$. Furthermore, the IR drop of SC-TC-2 was only about 0.04 V when at $5 \text{ A} \cdot \text{g}^{-1}$, implying a relatively low IR drop value for the supercapacitor.

The cycling stability of SC-TC-1, SC-TC-2 and SC-TC-3 was evaluated at $1 \text{ A} \cdot \text{g}^{-1}$. As seen in Figure 5c, SC-TC-2 can still maintain above 75% capacitance retention while undergoing 5000 charge-discharge cycles, indicating the ideal electrochemical stability. The last 10 charge/discharge curves (4991th-5000th cycles) of SC-TC-2 are displayed in Figure 5d. It can be obviously seen that all the GCD curves show almost symmetrical shapes.

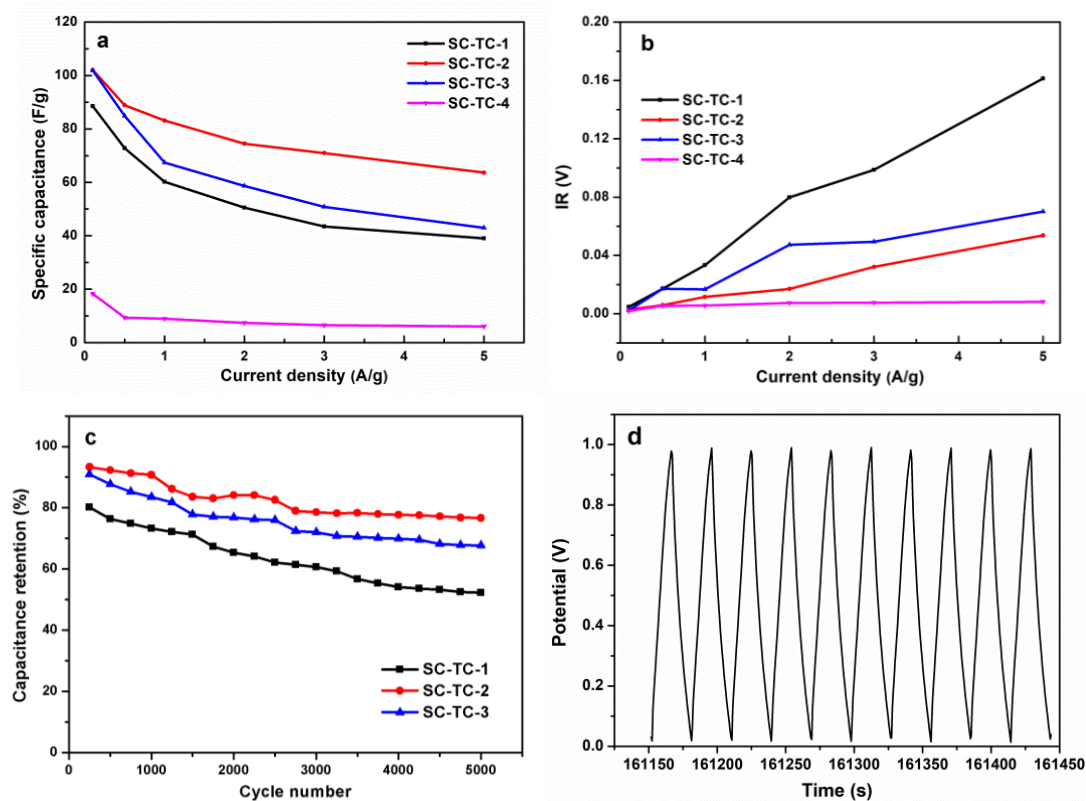


Figure 5. (a) Capacitive curves of SC-TCs at different current densities; (b) inner resistance variations as a function of the current density in SC-TCs; (c) cycle stability of SC-TCs at $1 \text{ A}\cdot\text{g}^{-1}$ over 5000 cycles; and (d) the last 10 charge/discharge curves of SC-TC-2 at $1 \text{ A}\cdot\text{g}^{-1}$ over 5000 cycles.

The capacitance calculated from the final cycles is about $59.6 \text{ F}\cdot\text{g}^{-1}$ at $1 \text{ A}\cdot\text{g}^{-1}$ for SC-TC-2, 76.7% of the initial value. These results indicate the good long-term capacitance retention of SC-TC-2 during the cycle test should be ascribed to its highest specific surface area and unique porous structure.

EIS is a powerful tool to investigate the relationship between the electrochemical properties and structure of the electrode materials [31,32]. The EIS spectra of SC-TCs were measured in the frequency range from 0.01 Hz to 100 kHz with an AC perturbation of 5 mV, as shown in Figure 6a and their enlarged plot curves displayed in Figure 6b. It can be observed that all the Nyquist plots of four tested samples exhibited similar shapes with an arc seen in the high frequency region, a Warburg resistance (Z_w) section of 45° in the middle frequency, and a straight line in lower frequency region. The left plot intersection at the real part (Z') in the high frequency range was associated with the square resistance and electrolyte resistance (R_s) of SC-TCs. The arc region in the plot curve for each SC-TC represents the charge transfer resistance (R_c), indicating the migration rate of hydrated K^+ and OH^- ions in SC-TCs at the interface between the electrode surface and solution. Moreover, it can be noticed that the Z_w section was very short for all the SC-TCs, suggesting an effective access of ions and an ideally short diffusion pathway to the TC-based electrode surface. A greater slope of the low frequency line usually suggests the material closer to an ideal supercapacitor with good electrocapacitive behavior [33]. Furthermore, the arc diameter of SC-TC-2 was smaller, comparatively,

indicating the lower charge-transfer resistance. And the slope of SC-TC-2 exhibited almost a straight line in lower frequency, implying the enhanced accessibility of the ions.

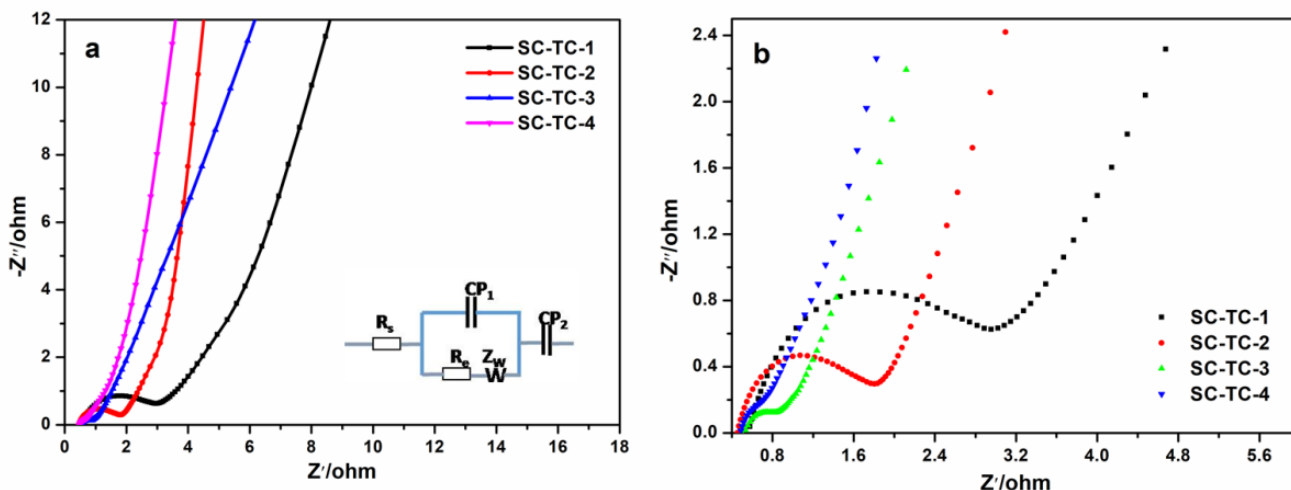


Figure 6. (a) Nyquist plots of SC-TCs in the frequency range of 0.01 Hz to 100 kHz under open circuit potential conditions and (b) the magnified profile. The inset in (a) is the equivalent circuit of Nyquist plots.

4. CONCLUSIONS

Four hierarchical porous carbon materials were prepared based on tib via carbonization at controlled temperatures. All TCs possessed mainly microporous structure. The results show TC-2 displayed the best electrochemical performance among all TC samples with the largest specific surface area, of which the specific capacitance was $102.1 \text{ F}\cdot\text{g}^{-1}$ at $0.1 \text{ A}\cdot\text{g}^{-1}$ in symmetrical two-electrode cells. TC-2-based supercapacitor maintained about 77% after 5000 charge-discharge cycles at $1 \text{ A}\cdot\text{g}^{-1}$. Our results provide a novel and facile way by utilizing synthesized benzene-contained organic compounds for the preparation of hierarchical porous carbons through rational design and indicate tib can be an ideal carbon precursor.

ACKNOWLEDGMENTS

This work was supported by the National Natural Science Foundation of China (Grant No. 51773102); and the Qingdao Postdoctoral Application Research Project (Grant No. 2015134).

References

1. L.L. Zhang, X.S. Zhao, *Chem. Soc. Rev.*, 38 (2009) 2520.
2. G.P. Wang, L. Zhang, J.J. Zhang, *Chem. Soc. Rev.*, 41 (2012) 797.
3. J.T. Zhang, J.W. Jiang, H.L. Li, X.S. Zhao, *Energ. Environ. Sci.*, 4(2011) 4009.
4. Z.C. Li, K.L. Zhai, G.Q. Wang, Q. Li, P.Z. Guo, *Materials*, 9 (2016) 912.
5. C.G. Liu, Z.N. Yu, D.Neff, A. Zhamu, B.Z.Jang, *Nano Lett.*, 10 (2010) 4863.

6. C. Largeot, C. Portet, J. Chmiola, P.L. Taberna, Y. Gogotsi, P. Simon, *J. Am. Chem. Soc.*, 130 (2008) 2730.
7. Y. Zhang, H. Feng, X.B. Wu, L.Z. Wang, A.Q. Zhang, T.C. Xia, H.C. Dong, X.F. Li, L.S. Zhang, *Int. J. Hydrogen Energ.*, 34 (2009) 4889.
8. G. Hasegawa, *Studies on porous monolithic materials prepared via sol-gel processes*, Springer, (2012) Berlin, Germany.
9. J.R. Miller, P. Simon, *Science*, 321(2008) 651.
10. J. Chmiola, G. Yushin, Y. Gogotsi, C. Portet, P. Simon, P.L. Taberna, *Science*, 313 (2006) 1760.
11. R. Lin, P.L. Taberna, J. Chmiola, D. Guay, Y. Gogotsi, P. Simon, *J. Electrochem. Soc.*, 156 (2009) A7.
12. B. Hou, T. Zhang, R.W. Yan, D. Li, Y. Mo, L.H. Yin, Y. Chen, *Int. J. Eelectrochem. Sci.*, 11 (2016) 9007.
13. S.B. Liu, Z.C. Li, X.X. Wang, X.H. Liu, W.N. Ye, Y.Z. Long, H.L. Li, P.Z. Guo, X.S. Zhao, *Int. J. Eelectrochem. Sci.*, 12 (2017) 11244.
14. A. Fuertes, G. Lota, T. Centeno, E. Frackowiak, *Electrochim. Acta*, 50 (2005) 2799.
15. Z.C. Li, G.Q. Wang, K.L. Zhai, C.C. He, Q. Li, P.Z. Guo, *Coll. Surf. A*, 538 (2018) 28.
16. P.Z. Guo, Q.Q. Ji, L.L. Zhang, S.Y. Zhao, X.S. Zhao, *Acta Phys-Chim. Sin.*, 27 (2011) 2836.
17. J. Fan, L. Gan, H. Kawaguchi, W.Y. Sun, K.B. Yu, W.X. Tang, *Chem. Eur. J.*, 9 (2003) 3965.
18. R.F. Wu, T.L. Zhang, X.J. Qiao, *Chin. Chem. Lett.*, 21(2010) 1007.
19. Y.L. Li, J.A. Hua, Zhao, Y. Y.S. Kang, W.Y. Sun, *Micropor. Mesopor. Mat.*, 214 (2015) 188.
20. Y.J. Jeong, K.H. Lee, K.A. Kim, S.H. Kim, *Materials*, 9 (2016) 995.
21. M.D. Stoller, R.S. Ruoff, *Energ. Environ. Sci.*, 3 (2010) 1294.
22. S. Brunauer, *The adsorption of gases and vapours*, Princeton University Press, (1945) Princeton, USA.
23. X.L. Li, C.L. Han, X.Y. Chen, C.W. Shi, *Micropor. Mesopor. Mat.*, 131 (2010) 303.
24. Y.T. Luan, L. Wang, S.E. Guo, B.J. Jiang, D.D. Zhao, H.J. Yan, C.H. Tian, H.G. Fu, *Rsc Adv.*, 5 (2015) 42430.
25. K. Le Van, T.T.L. Thi, *Prog. Nat. Sci-Mater.*, 24 (2014) 191.
26. H. Chen, Y.C. Guo, F. Wang, G. Wang, P.R. Qi, X.H. Guo, B. Dai, F. Yu, *New Carbon Mater.*, 32 (2017) 592.
27. F. Barzegar, A. Bello, J.K. Dangbegnon, N. Manyala, X.H. Xia, *Appl. Energ.*, 207 (2017) 417.
28. N.S.M. Nor, M. Deraman, M. Suleman, M.R.M. Jasni, J.G. Manjunatha, M.A.R. Othman, S.A. Shamsudin, *Int. J. Electrochem. Sci.*, 12 (2017) 2520.
29. R. Farma, M. Deraman, Awitdrus, I.A. Talib, R. Omar, J.G. Manjunatha, M.M. Ishak, N.H. Basri, B.N.M. Dolah, *Int. J. Electrochem. Sci.*, 8 (2013) 257.
30. M. Inada, N. Enomoto, J. Hojo, K. Hayashi, *Adv. Power Technol.*, 28 (2017) 884.
31. R.Y. Wang; Q. Li, L.L. Cheng, H.L. Li, B.Y. Wang, X.S. Zhao, P.Z. Guo, *Coll. Surf. A*, 457 (2014) 94.
32. X.J. He, J.W. Lei, Y.J. Geng, X.Y. Zhang, M.B. Wu, M.D. Zheng, *J. Phys. Chem. Solids*, 70 (2009) 738.
33. N. Roble, J. Ogbonna, H. Tanaka, *Appl. Microbiol. Biot.*, 60 (2003) 671.